Photo response of ^{164}Dy

O. Papst,[1,*] V. Werner,[1,2] J. Isaak,[1] N. Pietralla,[1] T. Beck,[1] C. Bernards,[2] M. Bhike,[3] N. Cooper,[2,†] B. P. Crider,[4,‡] U. Friman-Gayer,[1,§] J. Kleemann,[1] Krishichayan,[3] B. Löher,[5] F. Naqvi,[2,‖] E. E. Peters,[6] F. M. Prados-Estévez,[4,6] R. S. Ilieva,[2,7] T. J. Ross,[6] D. Savran,[5] W. Tornow,[3] and J. R. Vanhoy[8]

[1]*Institut für Kernphysik, Technische Universität Darmstadt, 64289 Darmstadt, Germany*
[2]*Wright Nuclear Structure Laboratory, Yale University, New Haven, Connecticut 06520, USA*
[3]*Department of Physics, Duke University, Durham, North Carolina 27708-0308, USA and Triangle Universities Nuclear Laboratory, Durham, North Carolina 27708-0308, USA*
[4]*Department of Physics and Astronomy, University of Kentucky, Lexington, Kentucky 40506-0055, USA*
[5]*GSI Helmholtzzentrum für Schwerionenforschung GmbH, 64291 Darmstadt, Germany*
[6]*Department of Chemistry, University of Kentucky, Lexington, Kentucky 40506-0055, USA*
[7]*Department of Physics, University of Surrey, Guildford, GU2 7XH, United Kingdom*
[8]*Department of Physics, United States Naval Academy, Annapolis, Maryland 21402-5026, USA*

(Received 22 April 2020; accepted 2 September 2020; published 21 September 2020)

Background: Little data is available for the pygmy dipole resonance (PDR) in axially deformed nuclei. Photon-scattering experiments are complicated by high level densities in the PDR region and the small energy difference of transitions to the ground state and to excited states.
Purpose: We report on an experimental study of the low-energy dipole strength distribution of the well-deformed nucleus ^{164}Dy between 4.0–7.7 MeV.
Methods: The low-lying photoresponse of ^{164}Dy has been investigated using the method of nuclear resonance fluorescence using a quasimonochromatic linearly polarized γ-ray beam in the energy range of 4.0–7.7 MeV in steps of 0.2 MeV.
Results: For excitation energies between 4 MeV and 5 MeV, sufficiently low level densities allow for the identification of individual states, including level energies, reduced transition widths and branching ratios. Energy-averaged mean decay branching ratios, mean population ratios and partial absorption cross sections were determined above 5 MeV up to the neutron-separation threshold at 7.7 MeV. A Lorentzian-shaped enhancement of the partial photo absorption cross section followed by decays back to the ground-state band is found at 6.10(5) MeV with a width of 0.77(23) MeV. A comparison with results from complementary measurements is performed using the framework of the statistical model.
Conclusions: The experimental results for the mean population ratios deviate systematically from the statistical model simulation by 30(6)%. However, they are in agreement within one standard deviation of the simulation.

DOI: 10.1103/PhysRevC.102.034323

I. INTRODUCTION

The electric dipole ($E1$) response of nuclei is dominated by the isovector giant dipole resonance (IVGDR) [1,2], discovered in 1937 by Bothe and Gentner [3] and systematically studied by Baldwin and Klaiber [4]. For spherical nuclei, its shape resembles a Lorentzian distribution, above the neutron separation threshold, with a centroid energy of about 15 MeV for heavy nuclei, and about 24 MeV for light nuclei [5]. In statically deformed nuclei, a splitting of the IVGDR into two components corresponding to oscillations parallel ($K = 0$) and perpendicular ($K = 1$) to the symmetry axis of the nucleus has been observed [6–9]. Here, K is the projection of the angular momentum quantum number on the intrinsic symmetry axis. The resulting strength distribution can be described as a superposition of two Lorentzian distributions. Should triaxial deformation be present, the $E1$ distribution may even separate into three Lorentzians [10,11].

On the low-energy end of the IVGDR in the vicinity of the neutron separation threshold, an enhancement of dipole strength over the Lorentzian extrapolation of the IVGDR has been observed for many nuclei [12–14]. This so-called pygmy dipole resonance (PDR) is often interpreted in a geometrical picture as an out-of-phase oscillation of a neutron skin against

*opapst@ikp.tu-darmstadt.de
†Deceased.
‡Present address: Department of Physics and Astronomy, Mississippi State University, Starkville, Mississippi 39762, USA.
§Present address: Department of Physics and Astronomy, University of North Carolina at Chapel Hill, Chapel Hill, North Carolina 27599, USA, and Triangle Universities Nuclear Laboratory, Durham, North Carolina 27708-0308, USA.
‖Present address: Department of Physics and Astrophysics, University of Delhi, Delhi 110007, India.

an isospin saturated core, while alternative interpretations refer to possible toroidal character [15] or α clustering [16,17]. Similarly to the IVGDR, a sensitivity of the PDR to the nucleus' symmetry axes is expected, suggesting the possibility of a similar kind of K splitting for deformed nuclei [18,19]. However, the evolution of the PDR for deformed nuclei is still barely investigated and significant experimental evidence for K splitting of the PDR is missing [20,21].

The magnetic part of the low-lying dipole response in deformed atomic nuclei is primarily composed of the scissors mode and the spin-flip mode. The scissors mode [22–24], discovered experimentally in 1983 by Bohle *et al.* [25], results in a concentration of orbital dipole strength located around 3 MeV for rare-earth nuclei. It is associated with a collective relative motion of a set of valence neutrons and protons against each other.

For rare-earth nuclei, the spin-flip resonance [24] is usually found in the energy region of 5–10 MeV. Its existence can be motivated in a shell-model picture: A single-particle transition between two orbitals with the same orbital angular momentum l, but opposing spin orientation results in a change of the spin quantum number ($\Delta S = 1$) and total angular momentum quantum number ($\Delta J = 1$), but no change in orbital angular momentum ($\Delta L = 0$). For even-even nuclei with a 0^+ ground state, this results in $J^\pi = 1^+$ states with strong corresponding magnetic dipole transitions due to the usually large spin g factors. Its excitation energy is related to the average spin-orbit splitting.

This paper reports on the experimental investigation of the dipole response of ^{164}Dy. With a quadrupole deformation parameter of $\beta = 0.3486(21)$ [26], it features one of the most pronounced ground-state deformations found for stable rare-earth nuclei. Hence, it is a possible candidate for the observation of the energy splitting of the PDR due to deformation. In previous photoexcitation measurements by Wesselborg *et al.* [27] and Margraf *et al.* [28], ^{164}Dy was probed up to excitation energies of 4 MeV. In the photon-scattering experiments presented in this work, excitation energies ranging from 4.0 MeV to slightly below the neutron separation threshold at 7.7 MeV have been probed with real photons for the first time.

II. EXPERIMENTAL METHOD

The photoresponse of ^{164}Dy was studied using the method of nuclear resonance fluorescence (NRF) [29]. The experiment was performed at the High Intensity γ-ray Source HIγS [30]. It provides quasimonochromatic linearly polarized γ-ray beams produced from laser Compton backscattering of free-electron laser photons off ultrarelativistic electrons. The resulting γ-ray beam was collimated by a cylindrical lead collimator with a diameter of 19.05 mm. The typical bandwidth of the collimated γ-ray beam, described by the full width at half-maximum (FWHM) of its energy spectrum, is about 3% of the beam centroid energy with a typical peak photon flux of $10^2\ \gamma/(\mathrm{s\,eV})$ on target.

A combination of two targets was used that were placed behind one another in an evacuated beam pipe. The first target consisted of 98% enriched $^{164}\mathrm{Dy}_2\,\mathrm{O}_3$ with a total mass of 770 mg. The second target, 95.6% enriched metallic ^{164}Dy, had a mass of 1.1 g.

For the detection of the γ radiation, the γ^3 setup [31] at HIγS was utilized. It was equipped with four high-purity germanium (HPGe) detectors with a relative efficiency of 55% compared to a standard NaI detector at 1.33 MeV. The detectors were arranged around the target position with distances ranging from 7–12 cm. Their orientations are specified using azimuthal (ϑ) and polar (φ) angles defined with respect to the horizontally polarized γ-ray beam. Two detectors were placed in the plane perpendicular to the direction of the γ-ray beam ($\vartheta = 90^\circ$), with one detector parallel ($\varphi = 0^\circ$) and one detector perpendicular ($\varphi = 90^\circ$) to the plane of polarization of the γ-ray beam. In addition, two detectors were placed at backward angles ($\vartheta = 135^\circ$ and $\varphi = 225^\circ, 315^\circ$). A further 123% HPGe detector, referred to as zero-degree detector, was moved into the path of the attenuated beam about 2.5 m downstream from the target position, in order to measure the spectral distribution of the beam. Measurements were performed with γ-ray beam energies ranging from 4.2–7.4 MeV in steps of 0.2 MeV, with measurement durations of about 5 h each up to 4.8 MeV and about 2 h each for higher beam energies.

Efficiency and energy calibrations were performed using ^{56}Co, ^{60}Co, and ^{152}Eu calibration sources [32–34]. To obtain reliable detection efficiencies for the studied γ-ray energy range, efficiency curves determined in GEANT4 [35–37] simulations (available in Ref. [38]) were scaled to the efficiency curves from the calibration measurements up to 3.5 MeV. Further energy calibration points at high energies were available from γ-ray beam measurements at 5.0 MeV and 7.4 MeV with a ^{11}B [39] target.

III. DATA ANALYSIS AND RESULTS

In the experimental spectra, it is possible to identify individual transitions at excitation energies of up to 5.0 MeV (see Fig. 1 as an example for $E_\gamma = 4.2$ MeV). At higher energies the obtained statistics are not sufficient to resolve individual peaks. Therefore, the data analysis consists of two parts that focus on the properties of individual states and the nucleus's average behavior in the energy range defined by the energy distribution of the γ-ray beam, respectively.

The estimation of uncertainties in this work follows the standards outlined by the Guide to the expression of uncertainty in measurement (GUM) [40]. Low statistics in the present work (e. g., refer to Fig. 1 or Fig. 5) result in large relative uncertainties that require a more general treatment of the propagation of uncertainties. Asymmetric uncertainties arise because of asymmetric probability distributions obtained in Monte Carlo calculations during uncertainty propagation [41]. For each calculation, the input quantities are resampled according to their assigned probability distribution. By repeatedly applying this method, a sample of the probability distribution of the output quantity can be determined. The numerical results stated in this work correspond to the mode of the determined probability distribution. Upper and lower errors indicate the boundaries of the shortest coverage interval which spans 68.3% of the calculated probability distribution.

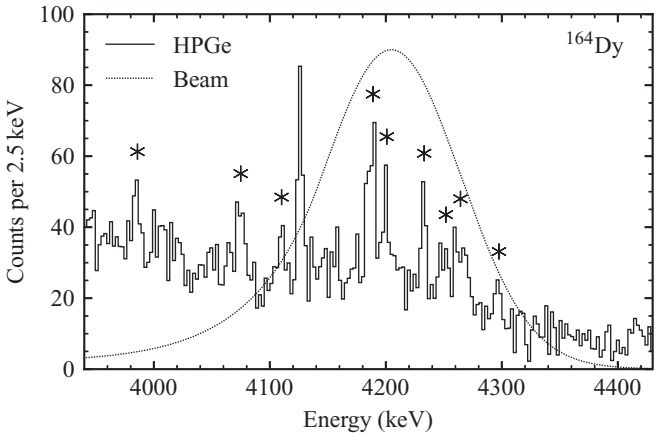

FIG. 1. The raw sum spectrum of all detectors is depicted for a γ-ray beam energy of 4.2 MeV. No background has been subtracted. Identified ground-state transitions are marked with an asterisk. The peak at 4127.4(6) KeV has been identified as the transition to the 2_1^+ state originating from the state at 4200.8(6) KeV. All states are newly observed, except for the one at $E_x = 3985.9(8)$ KeV. The dotted line shows the spectral distribution of the γ-ray beam.

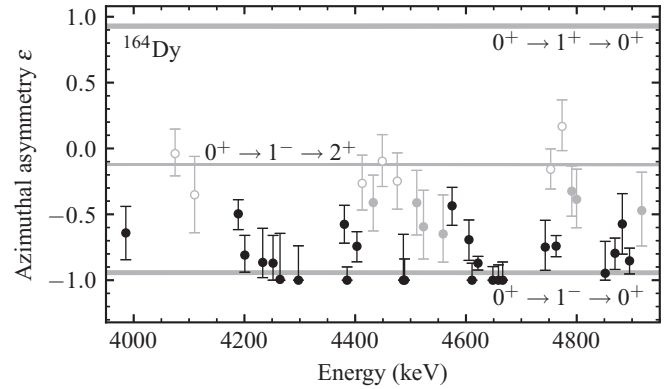

FIG. 2. Azimuthal asymmetries of ground-state transitions. For comparison, the simulated expected asymmetries for ground-state decays of 1^+ and 1^- states and decays of 1^- states to 2^+ states are shown in gray. Transitions marked with full circles ● correspond to ground-state decays of 1^- states. Transitions marked with open circles ○ do not allow for a conclusive parity assignment for the corresponding state. Transitions marked in gray (both open and full circles) could (within two standard deviations) have a significant probability of being caused by decays to the 2_1^+ state but are listed as ground-state transitions here.

A. State-by-state analysis

The excitation process in (γ, γ') photon-scattering experiments on atomic nuclei is especially selective to electric and magnetic dipole transitions [42]. Excitation energies E_x, partial and total transition widths Γ_k and Γ, branching ratios Γ_k/Γ_0, and energy-integrated scattering cross sections

$$I_{s,k} = \pi^2 \left(\frac{\hbar c}{E_x}\right)^2 g \frac{\Gamma_0 \Gamma_k}{\Gamma} \tag{1}$$

of excited states can be deduced in NRF experiments [29]. Here, k refers to the final state $J_k^{\pi_k}$.

For a fully linearly polarized γ-ray beam, as it is provided by HIγS, it is possible to distinguish electric and magnetic dipole-excited states because of the different angular distributions for ground-state transitions of even-even nuclei [43–45]:

$$W^{0^+\to 1^\pm \to 0^+}(\vartheta, \varphi) = \tfrac{3}{4}[1 + \cos(\vartheta)^2 \pm \cos(2\varphi)\sin(\vartheta)^2]. \tag{2}$$

In particular, the experimental azimuthal asymmetry [45]

$$\epsilon = P(E_\gamma) Q(E_\gamma) \Sigma = \frac{I_\parallel - I_\perp}{I_\parallel + I_\perp} \tag{3}$$

can be determined (see Fig. 2), where $P(E_\gamma)$ refers to the degree of polarization of the γ-ray beam with beam energy E_γ, Σ is the analyzing power of the nuclear reaction, and $Q(E_\gamma)$ is the polarization sensitivity of the experimental setup, which, in this case, is a geometrical factor that corrects for the finite solid angle and sensitivity of the setup. The photopeak-efficiency corrected γ-ray intensities in the detectors located either in the polarization plane of the incident γ-ray beam or perpendicular to it are given by $I_\parallel$ and $I_\perp$, respectively. An experimental asymmetry of 0.929(21) for ground-state transitions of $J^\pi = 1^+$ states and -0.943(17) for $J^\pi = 1^-$ states is expected from GEANT4 simulations for the geometry of the setup used in the present experiment for γ-ray beam energies below 5.0 MeV. The uncertainty of the expected asymmetries corresponds to the combination statistical and geometrical uncertainty of the performed simulation.

Although the statistics are not always sufficient, in most cases, the asymmetry is suggesting $J^\pi = 1^-$ states. Significant deviations from the expected asymmetry can be explained by overlapping transitions to the 2_1^+ state that are present in the same energy range. These overlapping transitions correspond to states that primarily decay to the 2_1^+ state at 73.393(5) KeV instead of the ground state, such that the ground-state transition is not observed in this work. Indeed, all states without parity quantum-number assignment in this work are located within the energy range where transitions to the 2_1^+ state may occur. A different approach to this problem is taken in Sec. III B, taking into account also unresolved strength.

For the calibration of the absolute photon flux that has been developed in Ref. [46] for a similar case, a three-step procedure was used. First, the spectral distribution of the γ-ray beam was determined using the zero-degree detector, which was placed in the (attenuated) γ-ray beam downstream of the experimental setup. To correct for the detector response of the HPGe detector, a deconvolution method was applied to obtain the energy profile from the experimental spectrum. The detector response was obtained in a GEANT4 simulation.

Next, the relative time- and energy-integrated photon flux was determined for each beam energy setting by a normalization based on the low-energy region of the spectra: The energy region of the experimental spectra below 1 MeV (see Fig. 3) is dominated by nonresonantly scattered radiation of the γ-ray beam that occurs in the target, but also other places where the beam collides with matter. The shape and relative intensity of this low-energy radiation can be related to the number of incident photons. The applicability of GEANT4 simulations for this purpose has been demonstrated in Refs. [46,47]. This has been explored and quantified using a GEANT4 simula-

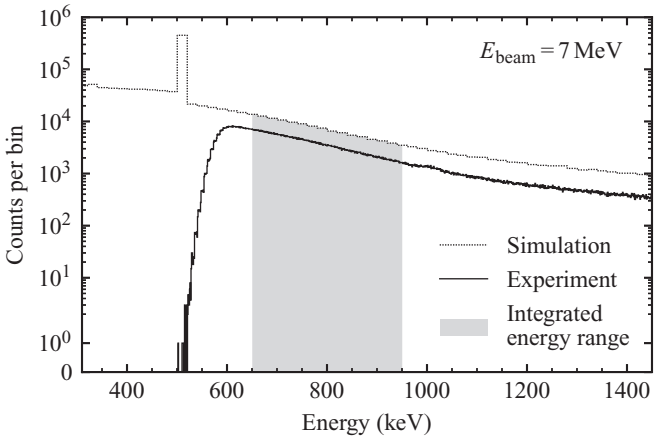

FIG. 3. Experimental and simulated spectrum of nonresonant scattering of γ rays into the HPGe detectors induced by an incident γ-ray beam with mean energy of 7 MeV. The energy range that is used for the relative photon flux calibration is highlighted. Natural background radiation was subtracted from the experimental spectrum and a hardware threshold was applied below 600 keV. The bin sizes are 1 keV and 20 keV, respectively, for the experimental and simulated spectrum. Comparison of the data to the simulation provides information on the incident photon flux.

tion [46,47]. This simulation approximates the γ-ray beam, assuming a circular profile with a diameter equivalent to the installed collimator. The energy distribution of the beam was approximated by a Gaussian distribution. An energy range between 650–950 keV was selected to study the low-energy scattering radiation (highlighted in gray in Fig. 3). The contributions from natural background radiation were eliminated by using time gates with respect to the pulsed γ-ray beam and by subtracting natural background spectra. The ratio of the area of the selected energy range of the experiment to the simulation $N_\gamma^{\text{exp}}(E_\gamma)/N_\gamma^{\text{sim}}(E_\gamma)$ was determined for each beam energy setting. This ratio is used to normalize different beam settings with respect to live time and beam intensity by scaling the corresponding spectra. Thus, it was possible to normalize all measurements with different γ-ray beam energies relative to each other as demonstrated in Ref. [46].

To normalize the absolute energy-integrated cross sections for states observed in this experiment, the results from another experiment were used as a reference. The $J^\pi = 1^-$ state at 3985.9(8) KeV was observed both in this work and a previous NRF experiment using bremsstrahlung [28]. Since the photon-scattering cross section of this state was known from the literature, the procedure described above was applied for estimating the photon fluxes in all energy settings. Although, the decay branch of the 3985.9(8) KeV state to the 2_1^+ state, reported in Ref. [28], was not observed in the present work due to insufficient sensitivity because of too low photon flux at that energy, the existence of this decay branch was properly taken into account for the photon-flux estimates. Since the photon-scattering cross section of this state was known from the literature, the procedure described above was applied for estimating the photon fluxes in all energy settings. For a detailed description of the method, refer to Ref. [46].

All other states in this work were newly identified, and no further measurement of the state at 3985.9(8) KeV exists. The accuracy of the normalization of absolute energy-integrated cross sections and related absolute quantities is limited. For the present work, this state was located at the low-energy end of the spectral distribution of the γ-ray beam for the lowest beam energy setting of 4.2 MeV. Because of the necessary deconvolution procedure, the relative uncertainties on the low-energy tail of the spectral distribution of the γ-ray beam are close to one.

Similarly, for the NRF measurement using bremsstrahlung in Ref. [28], the energy of the state was close to the endpoint energy of 4.1 MeV. Thus, even a small fluctuation of the endpoint energy could have resulted in a significantly altered photon flux close to the endpoint energy. Consequently, the absolute normalization of all photoreaction cross sections determined here may be uncertain by a factor of about 2, while relative information is more precise. For both experiments, the state was only very weakly excited in consequence of the small photon flux at the excitation energy.

In addition to the ground-state transition also the transition to the 2_1^+ state was observed for several excited states, which allows us to determine the branching ratio $\Gamma_{2_1^+}/\Gamma_0$. Deviations of our data from the Alaga rules [48] can arise from mixing of states with $K = 0, 1$ into the wave functions of the excited states and can be addressed by two-state mixing [49,50] or potentially multistate mixing at higher level densities [51,52].

Furthermore, reduced transition strengths $B(\sigma L)\uparrow$ were determined. The experimental results for the state-by-state analysis are listed in Table I.

A sensitivity limit was defined to identify statistically the maximum intensity an unobserved transition could have in a spectrum. The uncertainty ΔN of the area N of a peak is given in first order by

$$\Delta N = \sqrt{N + N_{\text{bg}}}, \tag{4}$$

where N_{bg} corresponds to the number of background-related counts below the peak, which was obtained using a fit of a line-shape model. In this work, only peaks with a significance of three standard deviations were considered for newly observed states, i.e., $N/\Delta N \geqslant 3$.

B. Average quantities

To study the average behavior of the nucleus within the excitation energy range, the binning of the experimental spectra was reduced. The pulsed time structure of the γ-ray beam was used to suppress contributions from natural background radiation. Spectra were generated from in-beam and off-beam events using the available timing information. Then, the off-beam spectrum was subtracted from the on-beam spectrum, correcting for the length of the respective time windows. To correct for the detector response, a fit-based deconvolution method was applied to the spectra.

The low-energy $E_{2_1^+} = 73.393(5)$ KeV of the 2_1^+ state in comparison to the bandwidth of the γ-ray beam of about 300 KeV makes it challenging to separate transitions to this state from ground-state transitions in this approach. Still, for a similar experiment performed at HIγS by Tamkas *et al.*

TABLE I. States identified in ^{164}Dy. Measured level energies E_x, energy-integrated cross sections $I_{s,0_1^+}$ and experimental azimuthal asymmetries ϵ are listed. Using these quantities, transition widths $\Gamma_{0_1^+}$, $\Gamma_{2_1^+}$, branching ratios $\Gamma_{2_1^+}/\Gamma_{0_1^+}$, total angular momentum and parity quantum numbers J^π and transition strengths $B(\sigma 1)\uparrow$ were deduced. For states with uncertain parity assignment, both $B(E1)\uparrow$ and $B(M1)\uparrow$ are given. All states are newly observed, except for the one at 3985.9(8) KeV.

E_x (KeV)	$I_{s,0_1^+}$ [a] (eV b)	$\Gamma_{0_1^+}$ [a] (meV)	$\Gamma_{2_1^+}$ [a] (meV)	$\Gamma_{2_1^+}/\Gamma_{0_1^+}$	J^π	$B(\mathrm{E1})\uparrow$ [a] (10^{-5} e^2 fm^2)	$B(\mathrm{M1})\uparrow$ [a] (10^{-3} μ_N^2)	ϵ
3985.9(8)	6^{+3}_{-4}	9(5)	–	–	1^-	40(21)	–	−0.64(20)
4074.8(9)[b]	1.8(5)	2.5(7)	–	–	$1, 2^+$	10.7(28)	9.7(26)	−0.04(18)
4110.1(9)[b]	0.68(21)	0.99(31)	–	–	$1, 2^+$	4.1(13)	3.7(12)	−0.35(29)
4188.9(5)	0.84(10)	1.27(15)	–	–	1^-	5.0(6)	–	−0.50(12)
4200.8(6)	0.51(8)	3.1(7)	9^{+3}_{-4}	3.1(6)	1^-	12.2(27)	–	−0.81(14)
4233.06(34)	0.43(8)	0.67(13)	–	–	1^-	2.5(5)	–	$-0.86^{+0.26}_{-0.12}$
4251.7(11)	0.46(9)	0.72(14)	–	–	1^-	2.7(5)	–	$-0.87^{+0.21}_{-0.13}$
4264.3(13)	0.64(11)	1.01(18)	–	–	1^-	3.7(6)	–	$-0.99^{+0.35}_{-0.01}$
4297.5(8)	0.73(18)	1.17(29)	–	–	1^-	4.2(10)	–	$-1.00^{+0.26}_{-0.00}$
4380.5(10)	0.61(9)	3.6(8)	9^{+3}_{-4}	2.6(6)	1^-	12.3(26)	–	−0.58(14)
4385.5(11)	0.29(7)	0.49(12)	–	–	1^-	1.7(4)	–	$-1.00^{+0.10}_{-0.00}$
4403.2(4)	0.79(9)	4.2(7)	$9.0^{+2.2}_{-3.0}$	2.2(4)	1^-	14.1(23)	–	−0.74(12)
4412.6(6)[b]	0.30(7)	0.51(12)	–	–	$1, 2^+$	1.7(4)	1.5(4)	−0.26(21)
4432.6(10)[b]	0.40(9)	2.4(7)	$5.1^{+1.9}_{-2.9}$	2.5(7)	1^-	7.9(24)	–	−0.41(21)
4449.0(9)[b]	0.42(9)	0.72(15)	–	–	$1, 2^+$	2.4(5)	2.1(4)	−0.10(20)
4476.0(5)[b]	1.5(4)	2.6(7)	–	–	$1, 2^+$	8.4(21)	7.6(19)	−0.25(21)
4487.0(8)	1.32(34)	2.3(6)	–	–	1^-	7.3(18)	–	$-1.00^{+0.35}_{-0.00}$
4489.2(7)	0.72(15)	1.25(27)	–	–	1^-	4.0(9)	–	$-1.00^{+0.16}_{-0.00}$
4511.2(8)[b]	0.94(21)	1.7(4)	–	–	1^-	5.2(12)	–	−0.41(25)
4523.4(8)[b]	0.69(15)	$4.6^{+1.4}_{-2.0}$	4^{+2}_{-4}	1.7(10)	1^-	11(5)	–	−0.59(27)
4558.8(9)[b]	0.26(9)	0.47(15)	–	–	1^-	1.4(5)	–	$-0.65^{+0.30}_{-0.21}$
4575.0(5)	0.58(10)	3.4(9)	7^{+3}_{-4}	2.3(6)	1^-	10.3(26)	–	−0.44(15)
4605.5(7)	0.65(9)	5.3(10)	16(6)	3.4(6)	1^-	15.4(31)	–	−0.69(15)
4611.1(17)	0.43(8)	3.9(10)	14^{+5}_{-7}	3.9(9)	1^-	11.4(30)	–	$-1.00^{+0.13}_{-0.00}$
4621.79(19)	2.48(17)	8.1(7)	6.0(11)	0.76(9)	1^-	23.6(20)	–	−0.87(5)
4648.7(6)	0.82(11)	1.53(20)	–	–	1^-	4.4(6)	–	$-1.00^{+0.10}_{-0.00}$
4658.8(9)	0.62(10)	2.1(4)	1.7(6)	0.81(18)	1^-	6.0(11)	–	$-1.00^{+0.12}_{-0.00}$
4666.4(6)	0.79(12)	2.3(4)	1.2(4)	0.55(12)	1^-	6.6(11)	–	$-1.00^{+0.14}_{-0.00}$
4743.2(12)	0.35(8)	3.0(10)	10^{+4}_{-6}	3.5(11)	1^-	$8.2^{+2.3}_{-3.0}$	–	−0.75(19)
4753.0(8)[b]	0.48(7)	2.8(7)	$4.0^{+1.6}_{-2.3}$	2.0(6)	$1, 2^+$	7.4(18)	6.7(16)	−0.16(15)
4762.9(4)	1.18(10)	7.7(11)	18(5)	2.3(4)	1^-	20.4(29)	–	−0.74(8)
4773.6(10)[b]	0.31(5)	0.61(11)	–	–	$1, 2^+$	1.60(28)	1.45(25)	0.17(20)
4791.2(6)[b]	0.23(5)	0.45(10)	–	–	1^-	1.18(25)	–	−0.32(19)
4799.8(7)[b]	0.32(5)	0.64(11)	–	–	1^-	1.65(27)	–	−0.39(22)
4851.5(12)	0.35(7)	1.36(31)	$1.2^{+0.4}_{-0.6}$	$0.91^{+0.20}_{-0.25}$	1^-	3.4(8)	–	$-0.95^{+0.24}_{-0.05}$
4869.2(5)	0.77(10)	1.58(21)	–	–	1^-	3.9(5)	–	−0.80(12)
4882.4(9)	0.55(10)	1.8(4)	1.1(4)	$0.60^{+0.12}_{-0.16}$	1^-	4.5(10)	–	−0.57(23)
4895.5(5)	1.52(17)	4.1(5)	1.08(28)	0.28(5)	1^-	9.9(12)	–	−0.85(10)
4917.5(9)[b]	1.01(21)	2.7(6)	$0.65^{+0.22}_{-0.31}$	0.25(8)	1^-	6.4(14)	–	−0.47(28)

[a]Absolute quantities were normalized using the state at 3985.9(8) KeV previously observed in bremsstrahlung experiments by Margraf *et al.* [28]. In addition to the statistical uncertainties given in the table, the normalization procedure results in an additional uncertainty of 56% that has to be added quadratically. See discussion for the reliability of the results.

[b]It can not be excluded by two standard deviations that the corresponding line is caused by a transition to the 2_1^+ state instead, for which no corresponding ground-state transition was observed.

[46] probing the dipole strength of ^{156}Gd with $E_{2_1^+,^{156}\mathrm{Gd}} = 88.970(1)$ KeV, the separation of contributions related to decays to the 0_1^+ state and to the 2_1^+ state was possible using a fitting procedure. This kind of analysis assumes that the existing strength has no pronounced structure within the excitation energy range, i.e., the fragmentation of states is high. The resulting strength distribution then corresponds to the smooth shape of the beam profile both for transitions to the ground state and to other low-lying states. The sum of two curves with the shape of the spectral distribution of the beam were fitted to the experimental spectrum, with a shift of $E_{2_1^+}$ in between (refer to Fig. 4). Furthermore, the centroid energy of

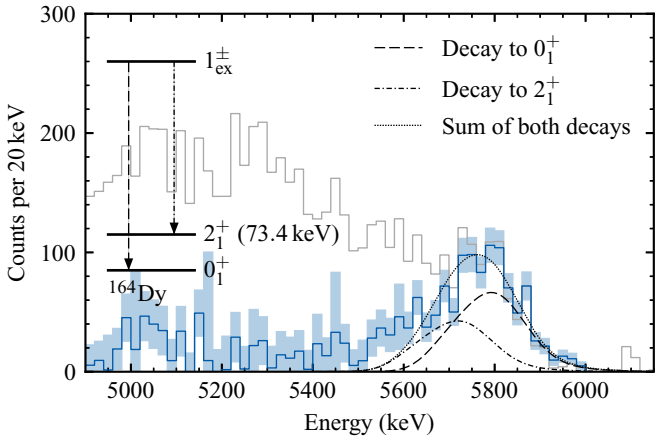

FIG. 4. Determination of mean branching ratios to the ground state and first 2^+_1 state for a beam energy of $E_{\text{beam}} = 5.8$ MeV. The original spectrum is shown in gray, the deconvoluted and background-corrected spectrum in blue, including an uncertainty band. Counts below the energy of the γ-ray beam correspond to the tail of the nonresonant scattering radiation.

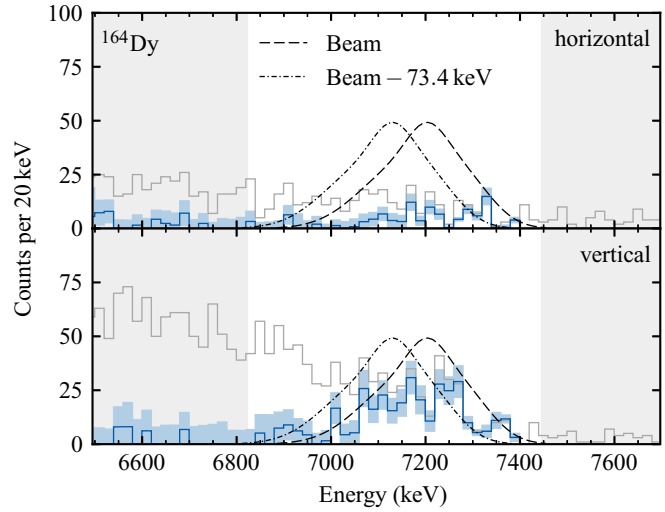

FIG. 5. Experimental spectra used for the determination of mean asymmetries for a beam energy of $E_{\text{beam}} = 7.2$ MeV. The top (bottom) spectrum belongs to the detector parallel (perpendicular) to the plane of polarization. For the determination of mean asymmetries, the highlighted region (white) was integrated. The original spectra are shown in gray, the deconvoluted and background-corrected spectra in blue. The energy distribution of the γ-ray beam is shown both at its original energy and shifted by $E_{2^+_1} = 73.393(5)$ KeV to highlight the energy regions, in which ground-state decays and decays to the 2^+_1 state are expected.

the resulting curve was chosen as a further free parameter. Due to low statistics, this procedure was applied to a sum spectrum of all detectors. This sum spectrum corresponds to a virtual detector that covers a large solid angle of the experimental setup. The solid angle coverage is such that the effects of the angular distribution of the emitted γ-ray radiation vanish almost completely [43,44].

In most cases, the centroid energy agreed with the measured beam energy by better than 5 KeV. But the large overlap of contributions from decays to the 0^+_1 state and to the 2^+_1 state prevented the visible distinction of two individual bumps, as it was possible for ^{156}Gd [46]. This is due to the lower energy of the 2^+_1 state of ^{164}Dy and the much lower statistics in the experimental spectra of the present experiment.

Mean asymmetries were determined for each energy range excited by the γ-ray beam by integration of the spectra. This is illustrated in Fig. 5. Ground-state transitions result in experimental asymmetries that are close to $\varepsilon \approx \pm 1$. Thus, the mean asymmetry for ground-state transitions can be used to determine the ratio of $E1$ to $M1$ strength in the excitation energy region. For $0^+ \rightarrow 1^{\pm} \rightarrow 2^+_1$ cascades, however, the γ radiation is emitted almost isotropically. Hence, the admixture of transitions to the 2^+_1 state that were present in this experiment attenuated the mean asymmetries to smaller absolute values. The results can be seen in Fig. 6. The observed mean asymmetries are in the range from $\langle\varepsilon\rangle = -0.4$ to $\langle\varepsilon\rangle = -0.7$, closer to the expected value for pure $E1$ transitions of $\langle\varepsilon_{\text{E1}}\rangle \approx -1$ than to the expected value for pure $M1$ transitions $\langle\varepsilon_{\text{M1}}\rangle \approx +1$. Because of the contributions from transitions to the 2^+_1 state, the absolute value of the measured mean asymmetries is reduced. The experimental results can be interpreted as lower limits for the absolute value of the asymmetry for ground-state transitions. Hence, it was found that $E1$ strength strongly dominates the studied energy region. This is further supported by the absence of 1^+ states with significant excitation widths Γ_0 in the energy range of 4–5 MeV that was found in the state-by-state analysis. Therefore, for this analysis, it was concluded that $M1$ strength can be neglected for the studied energy range.

Because of the uncertainty that is associated with the separation of contributions from decays to the 0^+_1 state and to the 2^+_1 state, a more robust definition of the mean branching ratios $\langle B_k\rangle$ was introduced, using the sum of both transitions to the ground state and to the 2^+_1 state in the energy region of interest

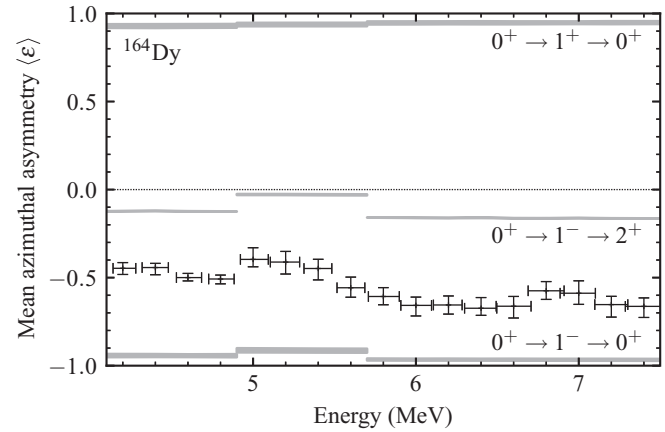

FIG. 6. Evolution of mean azimuthal asymmetries. For comparison, the simulated expected asymmetries for several cascades are shown in gray. Discontinuities of these simulated values are caused by different detector distances. The experimental asymmetries include both decays to the ground state and to the 2^+_1 state. Energy error bars correspond to the width (FWHM) of the γ-ray beam.

TABLE II. Mean branching ratios ($\langle B_k \rangle$) and mean population ratios ($\langle P_k \rangle$) for different excitation energies for ^{164}Dy.

E_{beam} (MeV)	$\langle B_{2_1^+} \rangle$[a]	$\langle B_{2_1^+} \rangle$[b]	$\langle P_{2_2^+} \rangle$	$\langle P_{3_1^+} \rangle$
4.2	$0.55^{+0.04}_{-0.04}$	$0.380^{+0.022}_{-0.024}$	–	–
4.4	$0.54^{+0.03}_{-0.05}$	$0.235^{+0.031}_{-0.025}$	–	–
4.6	$0.489^{+0.023}_{-0.030}$	$0.70^{+0.04}_{-0.04}$	–	–
4.8	$0.481^{+0.033}_{-0.028}$	$0.439^{+0.012}_{-0.011}$	–	–
5.0	$0.51^{+0.06}_{-0.07}$	$0.44^{+0.02}_{-0.04}$	–	–
5.2	$0.50^{+0.08}_{-0.07}$	$0.53^{+0.05}_{-0.06}$	–	–
5.4	$0.46^{+0.07}_{-0.06}$	$0.32^{+0.12}_{-0.12}$	–	–
5.6	$0.33^{+0.05}_{-0.07}$	$0.41^{+0.06}_{-0.04}$	–	–
5.8	$0.40^{+0.06}_{-0.06}$	$0.39^{+0.05}_{-0.03}$	$1.39^{+0.04}_{-0.08}$	–
6.0	$0.34^{+0.08}_{-0.05}$	$0.45^{+0.05}_{-0.05}$	$1.18^{+0.04}_{-0.06}$	–
6.2	$0.34^{+0.06}_{-0.06}$	$0.38^{+0.07}_{-0.05}$	$0.98^{+0.03}_{-0.05}$	$0.590^{+0.021}_{-0.031}$
6.4	$0.32^{+0.05}_{-0.07}$	$0.48^{+0.05}_{-0.05}$	$1.46^{+0.06}_{-0.08}$	$0.72^{+0.03}_{-0.04}$
6.6	$0.34^{+0.08}_{-0.06}$	$0.32^{+0.10}_{-0.08}$	$1.71^{+0.09}_{-0.07}$	$0.83^{+0.04}_{-0.03}$
6.8	$0.44^{+0.06}_{-0.07}$	$0.37^{+0.12}_{-0.07}$	$1.83^{+0.08}_{-0.08}$	$1.03^{+0.04}_{-0.05}$
7.0	$0.42^{+0.07}_{-0.09}$	$0.42^{+0.05}_{-0.04}$	$2.47^{+0.12}_{-0.13}$	$0.92^{+0.04}_{-0.05}$
7.2	$0.35^{+0.08}_{-0.06}$	$0.44^{+0.09}_{-0.07}$	$2.40^{+0.11}_{-0.13}$	$0.98^{+0.05}_{-0.05}$
7.4	$0.34^{+0.07}_{-0.06}$	$0.36^{+0.28}_{-0.09}$	$2.85^{+0.13}_{-0.17}$	$1.40^{+0.06}_{-0.08}$

[a]Determined using the mean asymmetry between the vertical and horizontal detector, assuming the absence of $M1$ strength.
[b]Determined using a fit to the sum spectrum of all detectors.

for normalization:

$$\langle B_k \rangle = \frac{\left\langle \frac{\Gamma_k}{\Gamma} \Gamma_{0_1^+} \right\rangle}{\left\langle \frac{\Gamma_{0_1^+}}{\Gamma} \Gamma_{0_1^+} \right\rangle + \left\langle \frac{\Gamma_{2_1^+}}{\Gamma} \Gamma_{0_1^+} \right\rangle} \tag{5}$$

$$= \frac{\langle I_{s,k} \rangle}{\langle I_{s,0_1^+} \rangle + \langle I_{s,2_1^+} \rangle} \tag{6}$$

$$= \frac{\sum_i I_{s,0_1^+ \to i \to k}}{\sum_i \left(I_{s,0_1^+ \to i \to 0_1^+} + I_{s,0_1^+ \to i \to 2_1^+} \right)}. \tag{7}$$

Mean branching ratios $\langle B_{2_1^+} \rangle$ to the 2_1^+ state were determined by two different methods: (i) from the fit procedure described above and (ii) from mean asymmetries. The number of counts

$$A^x \sim \langle B_{0_1^+} \rangle W_n^{0^+} + \langle B_{2_1^+} \rangle W_n^{2^+}, \tag{8}$$

observed in detector n in the energy region of the γ-ray beam can be related to the mean branching ratio with the angular distribution $W_n^{J^\pi}$ for the decay to the final J^π state for detector n. This quantity is obtained from a GEANT4 simulation and also takes into account the detection efficiency and finite solid angle coverage of the detector.

The results from both methods are listed in Table II. For excitation energies above 5.5 MeV, the results are found to be in good agreement within the experimental uncertainties. Below that energy, the results from the fit-based method deviate systematically from the asymmetry-based results. Because of the lower fragmentation of states, the assumption that the strength is distributed evenly within the excitation energy range may no longer be valid. The asymmetry-based method, however, does not rely on this assumption and is thus preferred for low excitation energies.

The decay of low-lying states of ^{164}Dy that were populated by decay cascades originating from excited states was observed for several beam energies. For beam energies of 5.8 MeV and above, the population of the 2_2^+ state at 762 KeV was observed, and for beam energies of 6.2 MeV and above, the population of the 3_1^+ state at 828 KeV was observed. The population of these low-lying states can be used to extract information about dipole strength in the PDR energy region [53].

The mean population ratio of a low-lying state $J_k^{\pi_k}$ from a photoexcited energy region is defined as the ratio of all decay chains originating from that region to the low-lying state relative to the direct decays to the ground-state band. It is accessible experimentally by the observation of depopulating transitions $J_k^{\pi_k} \to J_l^{\pi_l}$ of that low-lying state and can be expressed by

$$\langle P_k \rangle = \frac{\sum_{l=0}^{k-1} A^{k \to l} / \varepsilon(E_k - E_l)}{A^{x \to 0_1^+} / \varepsilon(E_x) + A^{x \to 2_1^+} / \varepsilon\left(E_x - E_{2_1^+}\right)}, \tag{9}$$

assuming isotropic angular distributions. The numerator sums over the efficiency-corrected intensities $A^{k \to l} / \varepsilon(E_k - E_l)$ of transitions of the low-lying state $J_k^{\pi_k}$, which is populated by decays originating from the photoexcited energy region, to all lower-lying states up to $J_{k-1}^{\pi_{k-1}}$. For the low-lying 2_2^+ state at 762 KeV and the 3_1^+ state at 828 KeV, the transition at 762 KeV ($2_2^+ \to 0_1^+$) and 755 KeV ($3_1^+ \to 2_1^+$) are observed, respectively. Unobserved decays to other lower-lying states are corrected for using the known branching ratios from literature [54]. The denominator is the sum of the efficiency-corrected intensities of decays from photoexcited states $J_x^{\pi_x}$ to the ground state band, i.e., the 0_1^+ and 2_1^+ states.

IV. DISCUSSION

A. States

In a proton-scattering experiment performed at the medium resolution spectrometer at TRIUMF, a 1^+ state was identified at 4.6 MeV [55] with a transition strength of $B(\text{M1})\uparrow = 0.27(4)\mu_N^2$. Total angular momentum and parity quantum numbers were assigned using the angular distribution. No such state was identified in this work. Rather, all states identified in the energy range of 4500–4700 keV were conclusively identified to be $J^\pi = 1^-$ states. Using the sensitivity limit determined in this work, a maximum transition strength of $B(\text{M1})\uparrow = 0.0007(4)\mu_N^2$ can be given for 4.6 MeV. This excludes the claim from Ref. [55] by at least two orders of magnitude.

B. Photon strength function

In a recent work by Renstrøm *et al.* [56], the photon strength function (PSF) and nuclear level density (NLD) of ^{164}Dy below the neutron separation threshold has been determined using the so-called Oslo method [57].

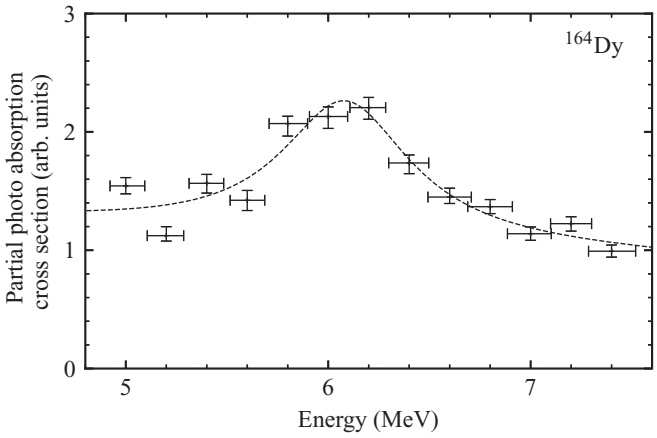

FIG. 7. Partial photoabsorption cross section, including only decays to the ground-state band. Energy error bars correspond to the width of the γ-ray beam. The dashed line depicts a fit of the SLO model on top of a linear background to the experimental results.

The extracted photon strength function includes contributions attributed to the IVGDR, the PDR and the scissors mode (SM):

$$f = f_{\mathrm{IVGDR1}} + f_{\mathrm{IVGDR2}} + f_{\mathrm{PDR1}} + f_{\mathrm{PDR2}} + f_{\mathrm{SM}}. \quad (10)$$

For the description of the PDR, the SLO model

$$f_{\mathrm{SLO}}(E_\gamma) = \frac{1}{3\pi^2\hbar^2c^2}\frac{\sigma_{\mathrm{SLO}}E_\gamma\gamma_{\mathrm{SLO}}^2}{\left(E_\gamma^2-\omega_{\mathrm{SLO}}^2\right)^2+E_\gamma^2\Gamma_{\mathrm{SLO}}^2}, \quad (11)$$

has been used [58], with resonance parameters (ω_{SLO}, σ_{SLO}, Γ_{SLO}). Renstrøm *et al.* [56] identify a concentration of strength located at $\omega_{\mathrm{PDR1}} = 6.33(14)$ MeV, $\Gamma_{\mathrm{PDR1}} = 1.9(3)$ MeV.

The PSF can be related to the photoabsorption cross section. A measurement of the photoabsorption cross section requires the observation of all decay branches of the excited states, which are not easily accessible in NRF experiments. An approximation can be obtained by combining ground-state decays and the observed decay of the 2_1^+ state, which is expected to collect cascades from higher-lying states [53,59]. In this work, the low-energy threshold in the acquisition of the γ-ray spectra prevented the decay of the 2_1^+ state at 73 KeV to be observed. Instead, an approximation of the photoabsorption cross section is obtained by only including decays to the ground-state band:

$$I \approx I_{s,0_1^+} + I_{s,2_1^+}. \quad (12)$$

In the following, this quantity will be referred to as partial photoabsorption cross section. The results can be seen in Fig. 7. A resonancelike structure is visible. By fitting the SLO model on top of a linear function to the experimental data, a centroid energy of $\omega_{\mathrm{PDR}} = 6.10(5)$ MeV and a width of $\Gamma_{\mathrm{PDR}} = 0.77(23)$ MeV were determined. The centroid energy is slightly lower in comparison to the Oslo results. The width is about 60% smaller for the results of the present work. No experimental evidence for a splitting of the PDR in ^{164}Dy built on the ground-state band is found within experimental uncertainties in the probed energy range.

The PSF and NLD determined in the Oslo experiment were used to perform a simulation in the framework of the statistical model (for the parameters used for the simulations discussed in the present work, refer to Table II– IV in Ref. [56]). The resulting branching ratios and population ratios were compared to the experimental results of this work.

A fundamental simplification usually assumed for statistical model calculations is the Brink-Axel hypothesis [60,61]. It states that the photon strength function between groups of nuclear states for a given multipole character only depend on the energy difference between initial and final states.

For the present work, a statistical model simulation code based on MCγ [62,63] was used, which is inspired by DICEBOX [64]. An extended reimplementation of the MCγ code was created that is able to track the population of low-lying states. The statistical model simulation code starts by generating a nuclear level scheme sampled from a level density model. At low excitation energies, where a nearly complete knowledge of all existing levels is assumed, the experimentally known level scheme is used. Next, for each generated level, transition strengths to all lower-lying states are sampled from a photon strength function model. Simultaneously, the resulting population of all lower-lying states is tracked following the excitation of each state, which allowed us to determine population ratios. Using a Monte Carlo method similar to the DICEBOX code [64], this procedure is performed multiple times. The repulsion of nuclear levels approximated by the Wigner distribution [65,66] and the empirically observed Porter-Thomas fluctuations of level widths [67] are taken into account. To account for the experimental uncertainties determined by Ref. [56], each Monte Carlo simulation uses a resampled parametrization of NLD and PSF according to the assigned probability distribution of each parameter.

A comparison of branching and population ratios from simulation and experiment is shown in Fig. 8. For the decay to the 2_1^+ state $\langle \mathrm{B}_{2_1^+}\rangle$, the simulation clearly underestimates the experimental results, which were determined from mean azimuthal asymmetries, by a factor of 2, especially for energies below 5.5 MeV. This deviation could be explained by a violation of the assumption that no contributions from $M1$ strength are present in this energy range. If ground-state transitions from 1^+ states are present, the number of counts for the horizontal detector that correspond to transitions to the 2_1^+ state is overestimated (see Fig. 6). Hence, significant $M1$ contributions would have resulted in an overestimation of mean branching ratios for the decay to the 2_1^+ state. However, as discussed above, the contributions of $M1$ excitations are so small that this effect cannot account quantitatively for the mismatch of data with the statistical model.

The population ratios for the 2_2^+ and 3_1^+ state are systematically underestimated by the simulation in comparison to the experimental data. The experimental population ratios for the 2_2^+ and 3_1^+ state are larger by an average factor of 1.33(7) and 1.28(8), respectively, resulting in a combined deviation of 30(6)%. However, both shape and slope of both population ratios are sufficiently reproduced and similar to each other. The experimentally observed decrease of the $\langle P_{2_2^+}\rangle$ population ratio as a function of increasing excitation energy below 6 MeV cannot be reproduced by the simulation.

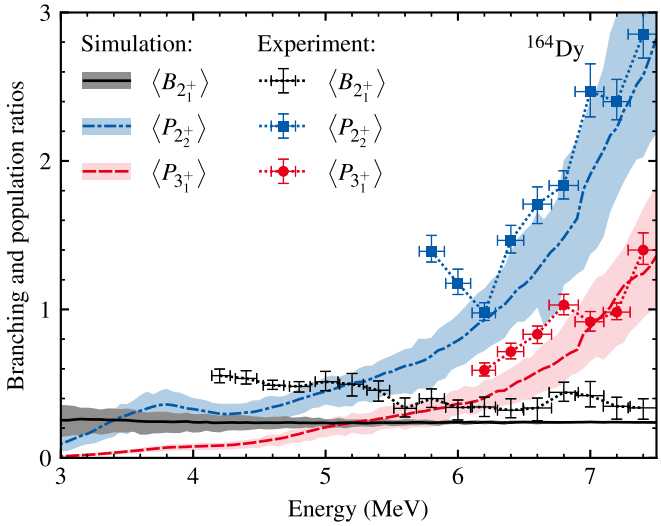

FIG. 8. Comparison statistical model simulation population and branching ratios. Energy error bars of the experimental values correspond to the width of the γ-ray beam. The experimental mean branching ratios were determined from mean azimuthal asymmetries, assuming the absence of $M1$ strength.

The $M1$ PSF that was used for the simulation is only based on the parametrization of the scissors mode by Renstrøm *et al*. [56] and does not include any contributions from the spin-flip resonance or a potential $M1$ upbend at low energies. Additional simulations with different parametrizations of the $M1$ PSF were performed. The inclusion of a spin-flip resonance using the SMLO $M1$ parametrization by Goriely and Plujko [68] has no significant influence on the population ratios, because its energy is too high to contribute to multistep cascades that result in the population of the 2_2^+ and 3_1^+ states. For this $M1$ PSF, the total strength of the scissors mode is the same, however, its width $\Gamma_{\rm sm}$ is increased. Combinatorically, this increases the probability for $E1$-$M1$ two-step cascades that result in the population of the 2_2^+ and 3_1^+ states. The results of this modified statistical model simulation are in better agreement with the experimental population ratios obtained in this work than the results of the unmodified statistical model simulation. Thus, the results of the present work indicate that the width of the scissors mode contribution to the $M1$ PSF is slightly underestimated by Renstrøm *et al*. [56].

V. CONCLUSION

The low-lying dipole strength of ^{164}Dy has been investigated using a quasimonochromatic γ-ray beam with γ-ray beam energies ranging from 4.2–7.4 MeV in steps of 0.2 MeV. Sufficiently low level densities allowed for a state-by-state analysis below 5.0 MeV. The absence of observed resolvable 1^+ states and the determined mean branching ratios indicate that the studied energy region is dominated by $E1$ strength.

The experimental results for the population ratios $\langle P_{2_2^+} \rangle$ and $\langle P_{3_1^+} \rangle$ are in good agreement with statistical model calculations based on experimental results by Renstrøm *et al*. [56] within 1σ. However, the simulation results are systematically smaller in comparison to the experiment. A better description of the experimental results can be obtained by using the SMLO $M1$ PSF by Goriely and Plujko [68] in combination with the $E1$ PSF from Ref. [56]. This can be attributed to the increased width of the scissors mode in the SMLO $M1$ PSF.

ACKNOWLEDGMENTS

We thank the HIγSoperators for providing excellent γ-ray beams for our experiment and M. Scheck and A. Zilges for valuable discussions. This work has been funded by the Deutsche Forschungsgemeinschaft (DFG, German Research Foundation) – Project-ID 279384907 – SFB 1245, by the State of Hesse under the grant "Nuclear Photonics" within the LOEWE program, by the BMBF under Grant No. 05P18RDEN9, and by the U.S. Department of Energy under Grants No. DE-FG02-91ER40609 and No. DE-FG02-97ER41033. T.B., U.F.-G., J.K., and O.P. acknowledge support by the Helmholtz Graduate School for Hadron and Ion Research of the Helmholtz Association. We would like to thank the former Wright Nuclear Structure Laboratory, Yale University, and the Institute for Nuclear Physics, University of Cologne, for providing the ^{164}Dy targets.

[1] J. Speth and A. van der Woude, Rep. Prog. Phys. **44**, 719 (1981).
[2] M. N. Harakeh and A. van der Woude, *Giant resonances: Fundamental High-Frequency Modes of Nuclear Excitation*, 1st ed., Oxford Studies in Nuclear Physics (Clarendon Press, Oxford, 2001), Vol. 24.
[3] W. Bothe and W. Gentner, Z. Phys. **106**, 236 (1937).
[4] G. C. Baldwin and G. S. Klaiber, Phys. Rev. **71**, 3 (1947).
[5] B. L. Berman and S. C. Fultz, Rev. Mod. Phys. **47**, 713 (1975).
[6] M. Danos, Nucl. Phys. **5**, 23 (1958).
[7] K. Okamoto, Phys. Rev. **110**, 143 (1958).
[8] E. G. Fuller and M. S. Weiss, Phys. Rev. **112**, 560 (1958).
[9] L. M. Donaldson, C. A. Bertulani, J. Carter, V. O. Nesterenko, P. von Neumann-Cosel, R. Neveling, V. Yu. Ponomarev, P.-G. Reinhard, I. T. Usman, P. Adsley, J. W. Brummer, E. Z. Buthelezi, G. R. J. Cooper, R. W. Fearick, S. V. Förtsch, H. Fujita, Y. Fujita, M. Jingo, W. Kleinig, C. O. Kureba, J. Kvasil, M. Latif, K. C. W. Li, J. P. Mira, F. Nemulodi, P. Papka, L. Pellegri, N. Pietralla, A. Richter, E. Sideras-Haddad, F. D. Smit, G. F. Steyn, J. A. Swartz, and A. Tamii, Phys. Lett. B **776**, 133 (2018).
[10] B. Bush and Y. Alhassid, Nucl. Phys. A **531**, 27 (1991).
[11] E. Grosse, A. R. Junghans, and R. Massarczyk, Eur. Phys. J. A **53**, 225 (2017).
[12] G. A. Bartholomew, Annu. Rev. Nucl. Sci. **11**, 259 (1961).
[13] D. Savran, T. Aumann, and A. Zilges, Prog. Part. Nucl. Phys. **70**, 210 (2013).
[14] A. Bracco, E. Lanza, and A. Tamii, Prog. Part. Nucl. Phys. **106**, 360 (2019).
[15] A. Repko, P.-G. Reinhard, V. O. Nesterenko, and J. Kvasil, Phys. Rev. C **87**, 024305 (2013).

[16] R. Bijker and F. Iachello, Phys. Rev. Lett. **112**, 152501 (2014).

[17] M. Spieker, S. Pascu, D. Bucurescu, T. M. Shneidman, T. Faestermann, R. Hertenberger, H.-F. Wirth, N.-V. Zamfir, and A. Zilges, Phys. Rev. C **97**, 064319 (2018).

[18] K. Yoshida and T. Nakatsukasa, Phys. Rev. C **83**, 021304(R) (2011).

[19] K. Yoshida and T. Nakatsukasa, Phys. Rev. C **88**, 034309 (2013).

[20] C. T. Angell, S. L. Hammond, H. J. Karwowski, J. H. Kelley, M. Krtička, E. Kwan, A. Makinaga, and G. Rusev, Phys. Rev. C **86**, 051302(R) (2012).

[21] P. M. Goddard, N. Cooper, V. Werner, G. Rusev, P. D. Stevenson, A. Rios, C. Bernards, A. Chakraborty, B. P. Crider, J. Glorius, R. S. Ilieva, J. H. Kelley, E. Kwan, E. E. Peters, N. Pietralla, R. Raut, C. Romig, D. Savran, L. Schnorrenberger, M. K. Smith, K. Sonnabend, A. P. Tonchev, W. Tornow, and S. W. Yates, Phys. Rev. C **88**, 064308 (2013).

[22] N. Lo Iudice and F. Palumbo, Phys. Rev. Lett. **41**, 1532 (1978).

[23] F. Iachello, Nucl. Phys. A **358**, 89 (1981).

[24] K. Heyde, P. von Neumann-Cosel, and A. Richter, Rev. Mod. Phys. **82**, 2365 (2010).

[25] D. Bohle, A. Richter, W. Steffen, A. E. L. Dieperink, N. Lo Iudice, F. Palumbo, and O. Scholten, Phys. Lett. B **137**, 27 (1984).

[26] B. Pritychenko, M. Birch, B. Singh, and M. Horoi, At. Data Nucl. Data Tables **107**, 1 (2016).

[27] C. Wesselborg, P. V. Brentano, K. O. Zell, R. D. Heil, H. H. Pitz, U. E. P. Berg, U. Kneissl, S. Lindenstruth, U. Seemann, and R. Stock, Phys. Lett. B **207**, 22 (1988).

[28] J. Margraf, T. Eckert, M. Rittner, I. Bauske, O. Beck, U. Kneissl, H. Maser, H. H. Pitz, A. Schiller, P. von Brentano, R. Fischer, R.-D. Herzberg, N. Pietralla, A. Zilges, and H. Friedrichs, Phys. Rev. C **52**, 2429 (1995).

[29] U. Kneissl, H. Pitz, and A. Zilges, Prog. Part. Nucl. Phys. **37**, 349 (1996).

[30] H. R. Weller, M. W. Ahmed, H. Gao, W. Tornow, Y. K. Wu, M. Gai, and R. Miskimen, Prog. Part. Nucl. Phys. **62**, 257 (2009).

[31] B. Löher, V. Derya, T. Aumann, J. Beller, N. Cooper, M. Duchene, J. Endres, E. Fiori, J. Isaak, J. Kelley, M. Knörzer, N. Pietralla, C. Romig, M. Scheck, H. Scheit, J. Silva, A. P. Tonchev, W. Tornow, H. Weller, V. Werner, and A. Zilges, Nucl. Instrum. Methods Phys. Res. A **723**, 136 (2013).

[32] H. Junde, H. Su, and Y. Dong, Nucl. Data Sheets **112**, 1513 (2011).

[33] E. Browne and J. K. Tuli, Nucl. Data Sheets **114**, 1849 (2013).

[34] M. J. Martin, Nucl. Data Sheets **114**, 1497 (2013).

[35] S. Agostinelli *et al.*, Nucl. Instrum. Methods Phys. Res. A **506**, 250 (2003).

[36] J. Allison *et al.*, IEEE Trans. Nucl. Sci. **53**, 270 (2006).

[37] J. Allison *et al.*, Nucl. Instrum. Methods Phys. Res. A **835**, 186 (2016).

[38] U. Friman-Gayer, J. Kleemann, and O. Papst, GEANT4 simulation of the Upstream Target Room (UTR) at the HIγS facility, 2019, available at https://github.com/uga-uga/utr.

[39] J. Kelley, E. Kwan, J. Purcell, C. Sheu, and H. Weller, Nucl. Phys. A **880**, 88 (2012).

[40] BIPM, IEC, IFCC, ISO, IUPAC, IUPAP, and OIML, *JCGM 100: Evaluation of Measurement Data – Guide to the Expression of Uncertainty in Measurement*, 1st ed. (Joint Committee for Guides in Metrology, Sèvres, 2008).

[41] BIPM, IEC, IFCC, ISO, IUPAC, IUPAP, and OIML, *JCGM 101: Evaluation of Measurement Data – Supplement 1 to the "Guide to the Expression of Uncertainty in Measurement" – Propagation of Distributions using a Monte Carlo Method*, 1st ed. (Joint Committee for Guides in Metrology, Sèvres, 2008).

[42] N. Pietralla, J. Isaak, and V. Werner, Eur. Phys. J. A **55**, 237 (2019).

[43] K. S. Krane, R. M. Steffen, and R. M. Wheeler, At. Data Nucl. Data Tables **11**, 351 (1973).

[44] R. M. Steffen and K. Alder, Angular distribution and correlation of gamma rays, in *The Electromagnetic Interaction in Nuclear Spectroscopy*, edited by W. D. Hamilton (North-Holland, Amsterdam, 1975), Chap. 12, pp. 505–582.

[45] N. Pietralla, Z. Berant, V. N. Litvinenko, S. Hartman, F. F. Mikhailov, I. V. Pinayev, G. Swift, M. W. Ahmed, J. H. Kelley, S. O. Nelson, R. Prior, K. Sabourov, A. P. Tonchev, and H. R. Weller, Phys. Rev. Lett. **88**, 012502 (2001).

[46] M. Tamkas, E. Aciksöz, J. Isaak, T. Beck, N. Benouaret, M. Bhike, I. Boztosun, A. Durusoy, U. Gayer, Krishichayan, B. Löher, N. Pietralla, D. Savran, W. Tornow, V. Werner, A. Zilges, and M. Zweidinger, Nucl. Phys. A **987**, 79 (2019).

[47] D. Savran and J. Isaak, Nucl. Instrum. Methods Phys. Res., Sect. A **899**, 28 (2018).

[48] G. Alaga, K. Alder, A. Bohr, and B. R. Mottelson, K. Dan. Vidensk. Selesk. Mat. Fys. Medd. **29**, 1 (1955).

[49] A. Zilges, P. von Brentano, A. Richter, R. D. Heil, U. Kneissl, H. H. Pitz, and C. Wesselborg, Phys. Rev. C **42**, 1945 (1990).

[50] T. Beck, V. Werner, N. Pietralla, M. Bhike, N. Cooper, U. Friman-Gayer, J. Isaak, R. V. Jolos, J. Kleemann, Krishichayan, O. Papst, W. Tornow, C. Bernards, B. P. Crider, R. S. Ilieva, B. Löher, C. Mihai, F. Naqvi, S. Pascu, E. E. Peters, F. M. Prados-Estevez, T. J. Ross, D. Savran, J. R. Vanhoy, and A. Zilges, Phys. Rev. Lett. **125**, 092501 (2020).

[51] N. Pietralla, P. von Brentano, R.-D. Herzberg, U. Kneissl, N. Lo Iudice, H. Maser, H. H. Pitz, and A. Zilges, Phys. Rev. C **58**, 184 (1998).

[52] D. Savran, S. Müller, A. Zilges, M. Babilon, M. W. Ahmed, J. H. Kelley, A. Tonchev, W. Tornow, H. R. Weller, N. Pietralla, J. Li, I. V. Pinayev, and Y. K. Wu, Phys. Rev. C **71**, 034304 (2005).

[53] M. Scheck, V. Yu. Ponomarev, T. Aumann, J. Beller, M. Fritzsche, J. Isaak, J. H. Kelley, E. Kwan, N. Pietralla, R. Raut, C. Romig, G. Rusev, D. Savran, K. Sonnabend, A. P. Tonchev, W. Tornow, H. R. Weller, and M. Zweidinger, Phys. Rev. C **87**, 051304(R) (2013).

[54] B. Singh and J. Chen, Nucl. Data Sheets **147**, 1 (2018).

[55] D. Frekers, D. Bohle, A. Richter, R. Abegg, R. E. Azuma, A. Celler, C. Chan, T. E. Drake, K. P. Jackson, J. D. King, C. A. Miller, R. Schubank, J. Watson, and S. Yen, Phys. Lett. B **218**, 439 (1989).

[56] T. Renstrøm, H. Utsunomiya, H. T. Nyhus, A. C. Larsen, M. Guttormsen, G. M. Tveten, D. M. Filipescu, I. Gheorghe, S. Goriely, S. Hilaire, Y.-W. Lui, J. E. Midtbø, S. Péru, T. Shima, S. Siem, and O. Tesileanu, Phys. Rev. C **98**, 054310 (2018).

[57] A. Schiller, L. Bergholt, M. Guttormsen, E. Melby, J. Rekstad, and S. Siem, Nucl. Instrum. Methods Phys. Res. A **447**, 498 (2000).

[58] R. Capote *et al.*, Nucl. Data Sheets **110**, 3107 (2009).

[59] J. Isaak, D. Savran, B. Löher, T. Beck, M. Bhike, U. Gayer, Krishichayan, N. Pietralla, M. Scheck, W. Tornow, V. Werner, A. Zilges, and M. Zweidinger, Phys. Lett. B **788**, 225 (2019).

[60] D. M. Brink, Ph.D. thesis, Oxford University, 1955, https://ora.ox.ac.uk/objects/uuid:334ec4a3-8a89-42aa-93f4-2e54d070ee09.
[61] P. Axel, Phys. Rev. **126**, 671 (1962).
[62] N. M. Cooper, Ph.D. thesis, Yale University, 2015, http://hdl.handle.net/10079/bibid/12890829.
[63] N. Cooper, C. W. Beausang, P. Humby, A. Simon, J. T. Burke, R. O. Hughes, S. Ota, C. Reingold, A. Saastamoinen, and E. Wilson, Phys. Rev. C **98**, 044618 (2018).
[64] F. Bečvàř, Nucl. Instrum. Methods Phys. Res. A **417**, 434 (1998).
[65] N. Rosenzweig and C. E. Porter, Phys. Rev. **120**, 1698 (1960).
[66] E. P. Wigner, Ann. Math. **62**, 548 (1955).
[67] C. E. Porter and R. G. Thomas, Phys. Rev. **104**, 483 (1956).
[68] S. Goriely and V. Plujko, Phys. Rev. C **99**, 014303 (2019).